

Article

New Coordination Compounds of Cu^{II} with Schiff Base Ligands—Crystal Structure, Thermal, and Spectral Investigations

Dariusz Osypiuk , Beata Cristóvão  and Agata Bartyzel * 

Department of General and Coordination Chemistry and Crystallography, Faculty of Chemistry, Institute of Chemical Sciences, Maria Curie-Skłodowska University in Lublin, Maria Curie-Skłodowska Sq. 2, 20-031 Lublin, Poland; dariusz.osypiuk@poczta.umcs.lublin.pl (D.O.); beata.cristovao@poczta.umcs.lublin.pl (B.C.)

* Correspondence: agata.bartyzel@poczta.umcs.lublin.pl

Received: 19 October 2020; Accepted: 4 November 2020; Published: 5 November 2020



Abstract: The new mono-, di- and tetranuclear coordination compounds [Cu(HL¹)]·H₂O (1), [Cu₂(L¹)(OAc)(MeOH)]·2H₂O·MeOH (2), [Cu₄(L²)₂(OAc)₂]·4MeOH (3), and [Cu₄(L²)₂(OAc)₂]·4H₂O·4MeOH (4) were synthesized by the direct reaction of 2,2'-(2-hydroxypropane-1,3-diyl)bis[nitrilomethylidene]bis(4-bromo-6-methoxyphenol) (H₃L¹) or 2,2'-(2-hydroxypropane-1,3-diyl)bis(nitriloeth-1-yl-1-ylidene)diphenol (H₃L²) and the Cu(II) salt. They were characterized by elemental analysis, X-ray fluorescence (XRF), Fourier transform infrared (FTIR) spectroscopy, simultaneous thermal analysis and differential scanning calorimetry (TG/DSC), and thermal analysis coupled with Fourier transform infrared spectroscopy (TG-FTIR) techniques and the single crystal X-ray diffraction study. In the dinuclear complex 2, the copper(II) ions are bridged by an alkoxo- and a carboxylato bridges. The tetranuclear complexes 3 and 4 are formed from dinuclear species linkage through the phenoxo oxygen atoms of the fully deprotonated H₃L². Compounds 1–4 are stable at room temperature. During heating in air, at first, the solvent molecules (water and/or methanol) are lost and after that, the organic part undergoes defragmentation and combustion. The final decomposition solid product is CuO. The main gaseous products resulting from the thermal degradation of 1–4 in a nitrogen atmosphere were: H₂O, MeOH, CH₃COOH, CH₄, C₆H₅OH, CO₂, CO, and NH₃.

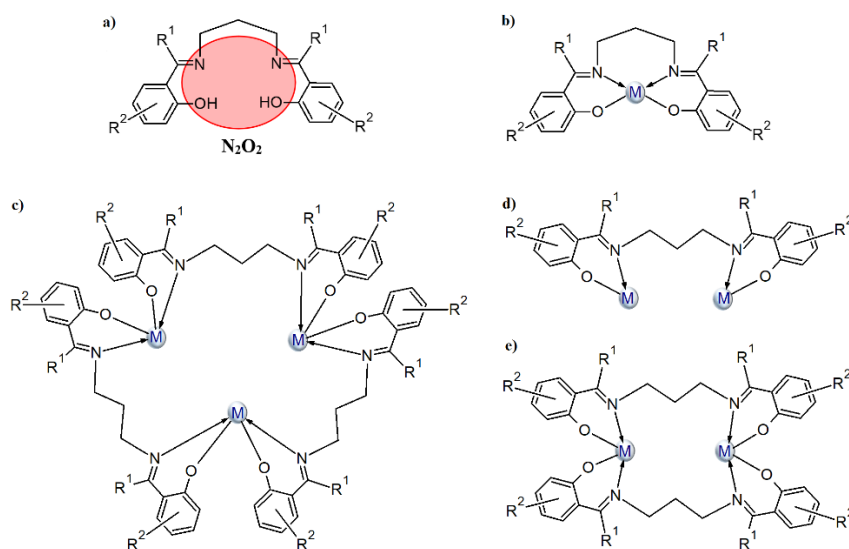
Keywords: Schiff base; N,O-donor ligand; complexes of Cu(II); crystal structure; thermal properties

1. Introduction

The interest in the N,O-donor Schiff bases in the field of coordination chemistry has increased over the last several years because they can form stable coordination compounds with most transition metals [1–21]. These types of ligands and their complexes show interesting properties that can be potentially used in various fields such as catalysis [7–9], analytical chemistry [10,11], magnetic [5,6,12–15], and photoluminescence materials [4,16–19], etc. They also exhibit significant biological properties (e.g., antifungal, antibacterial, antimalarial, antiproliferative, anti-inflammatory, antiviral, and antioxidant [1,4,20–26]).

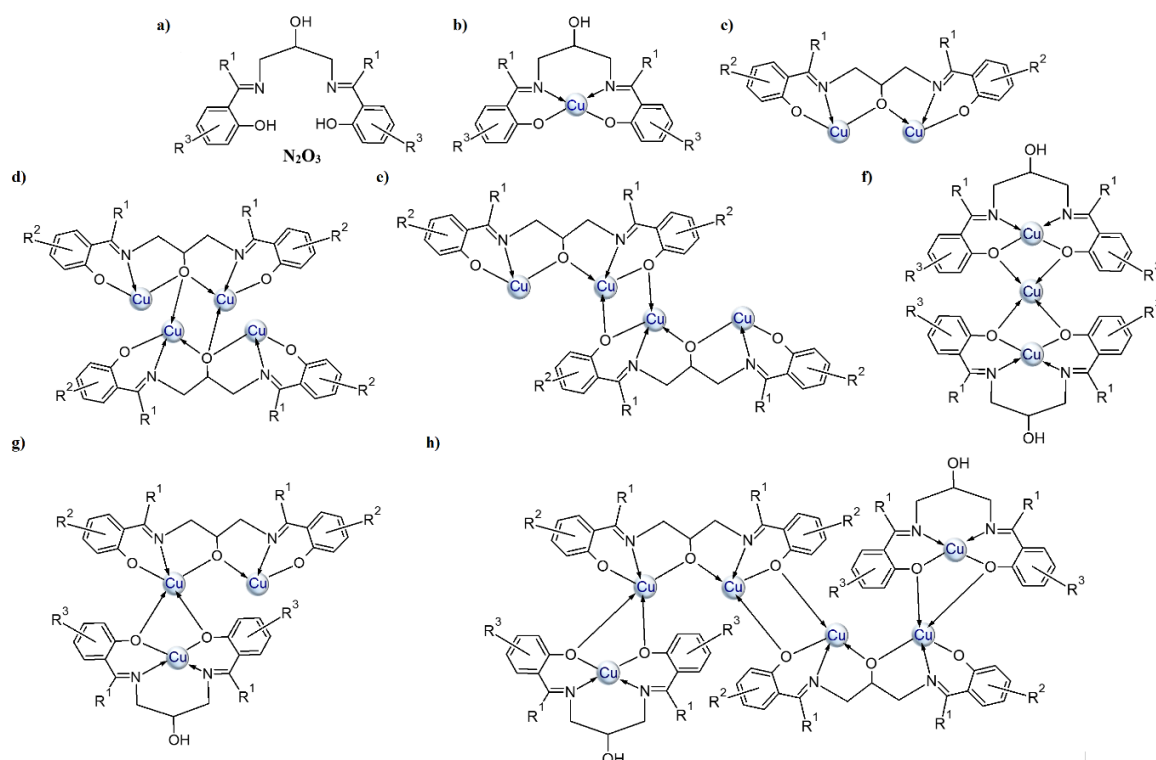
We are interested in the synthesis of Schiff bases based on aromatic aldehydes or ketones with flexible diamines (e.g., 1,3-diaminopropane) and the study of their coordination ability toward transition metal ions. Most Schiff bases, formed in reaction of 1,3-diaminopropane with *o*-hydroxy aromatic aldehydes/ketones (Scheme 1a), coordinate a single metal(II) ion in the N₂O₂ tetradentate cavity (Scheme 1b). The coordination environment of the metal ion consists of two oxygen and two nitrogen atoms of one Schiff base and occasionally, additional donor atoms derived from other molecules

(e.g., a solvent) are also present. Structures in which two metal ions are built into the cavity of the above-mentioned derivatives of the Schiff base are very rare. A survey of the Cambridge Structural Database (CSD version 5.41 with updates August 2020 [27] revealed that there is only one crystal structure where two metal(II) ions are incorporated into the N_2O_2 Schiff base cavity. This type of complex was obtained by Li et al. (CSD code: OBEFUW [27,28]) where the Schiff base ligand coordinates two Cd^{II} ions via one azomethine nitrogen and one phenolate oxygen atom (Scheme 1c). Additionally, the coordination sphere of metal centers is supplemented by two pyridine molecules. As a result, a metallomacrocyclic structure is formed. In the case of metal ions with a valence other than two, the above-mentioned type of ligand can also coordinate two metals via N_2O_2 donor atoms as depicted in Scheme 1 (CSD codes: HIYRIQ [27] (Scheme 1d) and ABULAN [27] and HUWNIW [27], Scheme 1e).



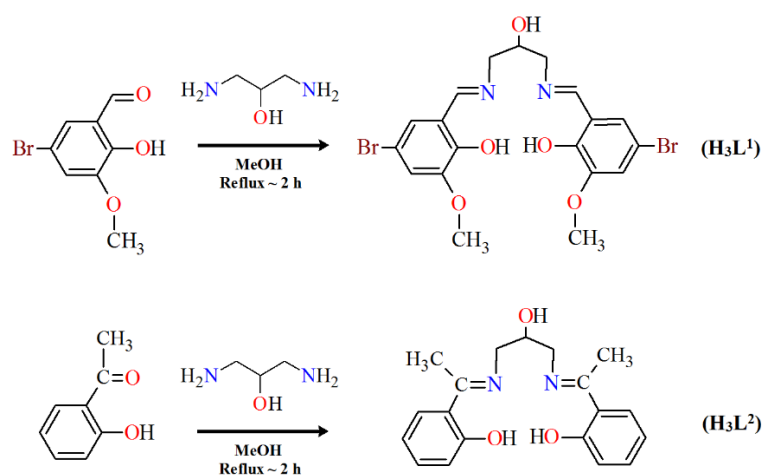
Scheme 1. The N_2O_2 -donor Schiff base ligands of 1,3-diaminopropane and *o*-hydroxy aromatic ketones/aldehydes (a) and their possible coordination modes (b–e).

In this paper, we present Cu^{II} complexes with similar types of ligands as depicted in Scheme 2a. The Schiff bases contain an additional hydroxyl group, which enhances their ability to coordinate more than one metal ion (see Scheme 2b–h and Table S1). According to the information found in the CSD database, two types of copper(II) ions coordination are most common (i.e., one ion is coordinated in the N_2O_2 cavity of the Schiff base (Scheme 2b) or when additional deprotonation of the alcoholic group occurs, two copper atoms are bound by N_2O_3 donor atoms of the ligand (Scheme 2c). Tetranuclear copper(II) complexes, where there is an additional oxygen atom either from the (Scheme 2d) alkoxide or phenoxide (Scheme 2e) group of the second Schiff base in the coordination environment of the central ion, are also quite often observed. Structures with a mixed type of coordination (Scheme 2g,h) are less common. Mukherjee et al. [29] synthesized cationic complexes consisting of a trinuclear copper(II) core (CSD codes: ILAPEQ [27] and ILAPIU [27]) where the coordination geometry of two terminal copper atoms was distorted square planar while the central ones had a distorted square-pyramidal. Yang and co-workers [30] also described a hexanuclear copper(II) complex (Scheme 2h).



Scheme 2. General depiction of the structures that bis *o*-hydroxy Schiff bases of 1,3-diamino-2-propanol and *o*-hydroxy aromatic ketones/aldehydes adopt with copper(II) ions: (a) imine ligand, (b–h) the possible coordination modes.

Herein, we report the crystal structures, thermal, and spectral properties of four new Cu(II) Schiff base complexes. In the research, we used two Schiff bases as ligands that differed in the amount and kind of substituents in the benzene ring (Scheme 3). 2,2'-((2-hydroxypropane-1,3-diyl) bis[nitrilomethylidene])bis(4-bromo-6-methoxyphenol) H₃L¹, possessing two imino nitrogen atoms, two phenolic oxygen atoms, one alcoholic oxygen atom, and two oxygen atoms of the methoxy groups, can potentially act as a seven-coordinated ligand. 2,2'-((2-hydroxypropane-1,3-diyl) bis(nitriloethyl-1-ylidene))diphenol H₃L² with two imino nitrogen and three oxygen (phenolic and alcoholic) atoms can react as a five-coordinated ligand.



Scheme 3. The route to the synthesis of H₃L¹ and H₃L².

2. Materials and Methods

2.1. Materials

The reagent grade chemicals (i.e., 1,3-diamino-2-propanol (97%), 5-bromo-2-hydroxy-3-methoxybenzaldehyde (98%), 2'-hydroxyacetophenon (99%), $\text{Cu}(\text{CH}_3\text{COO})_2 \cdot \text{H}_2\text{O}$ (98%), and methanol (99.8%)) were purchased from commercial sources and used as received without further purification.

2.2. Methods

Elemental analysis for C, H, and N was carried out using a CHN 2400 Perkin Elmer analyzer. The content of the copper was determined using an ED XRF spectrophotometer Canberra-Packard. The Fourier-transform infrared spectroscopy (FTIR) ($4000\text{--}400\text{ cm}^{-1}$) of 1, 2, and H_3L^1 was performed on a M-80 spectrophotometer Carl Zeiss Jena using KBr pellets. In the case of 3, 4, and H_3L^2 , the infrared spectra ($4000\text{--}520\text{ cm}^{-1}$) were recorded on a Thermo Scientific Nicolet 6700 FTIR equipped with a Smart iTR diamond ATR accessory with a resolution of 4 cm^{-1} for 16 scans. Thermal analysis of 1–4 was carried out by the thermogravimetric (TG, DTG) and differential scanning calorimetry (DSC) methods using the SETSYS 16/18 analyzer (Setaram). The experiments were carried out under air flow in the temperature range of $20\text{--}700\text{ }^\circ\text{C}$ at a heating rate of $10\text{ }^\circ\text{C}\cdot\text{min}^{-1}$. The samples of 5.99 mg (1), 7.74 mg (2), 5.24 mg (3), and 6.31 mg (4) were heated in Al_2O_3 crucibles. The TG–FTIR analysis of 1–4 was carried out using a TGA Q5000 analyzer TA Instruments, New Castle, Delaware, USA, interfaced to the Nicolet 6700 FTIR spectrophotometer (Thermo Scientific, Waltham, MA, USA). The samples of 1–4 were placed in an open platinum crucible and heated from ambient temperature to $700\text{ }^\circ\text{C}$ with a heating rate of $20\text{ }^\circ\text{C}\cdot\text{min}^{-1}$. Gas analysis was performed by matching the spectra against those from the spectrum library Nicolet TGA Vapor Phase of the software Ominic.

2.3. Synthesis

2.3.1. Synthesis of 2,2'-((2-hydroxypropane-1,3-diy)bis[nitrilomethylidene])bis(4-bromo-6-methoxyphenol) (H_3L^1)

The Schiff base H_3L^1 was synthesized from 5-bromo-2-hydroxy-3-methoxybenzaldehyde (2.31 g, 10 mmol) and 1,3-diamino-2-propanol (0.45 g, 5 mmol) in hot methanol (100 mL) according to the literature [31]. Yield 79%. *Anal.* (%) for $\text{C}_{19}\text{H}_{20}\text{Br}_2\text{N}_2\text{O}_5$ (MW: 516.18). Calcd: C, 44.21; H, 3.91; N, 5.43. Found: C, 44.10; H, 3.50; N, 5.00.

2.3.2. Synthesis of 2,2'-((2-hydroxypropane-1,3-diy)bis(nitriloeth-1-yl-1-ylidene))diphenol (H_3L^2)

The Schiff base H_3L^2 was synthesized from 2'-hydroxyacetophenon (1.36 g, 10 mmol) and 1,3-diamino-2-propanol (0.45 g, 5 mmol) in hot methanol (50 mL) according to the literature [3,32].

Yield 83%. *Anal.* (%) for $\text{C}_{19}\text{H}_{24}\text{N}_2\text{O}_4$ (MW: 344.40). Calcd: C, 66.26; H, 7.02; N, 8.13. Found: C, 66.20; H, 7.00; N, 8.40.

2.3.3. Synthesis of $[\text{Cu}(\text{HL}^1)] \cdot \text{H}_2\text{O}$ (1)

The 10 mL methanol solution of the copper(II) acetate (0.4 mmol, 0.0798 g) was drop-wise added to a hot solution of the Schiff base H_3L^1 (0.4 mmol, 0.2065 g) and the reaction mixture was stirred at a higher temperature ($\sim 45\text{ }^\circ\text{C}$) for about 30 min. The resulting solution was filtered off. Brown colored crystals resulted from the slow evaporation of the solution at low temperature ($\sim 6\text{ }^\circ\text{C}$).

Yield 45%, *Anal.* (%) for $\text{C}_{19}\text{H}_{19.5}\text{Br}_2\text{CuN}_2\text{O}_6$ (MW: 595.73). Calcd: C, 38.27; H, 3.27; N, 4.70; Cu, 10.66. Found: C, 38.10; H, 3.15; N, 4.50; Cu, 10.20.

2.3.4. Synthesis of $[\text{Cu}_2(\text{L}^1)(\text{OAc})(\text{MeOH})] \cdot 2\text{H}_2\text{O} \cdot \text{MeOH}$ (2)

Complex 2 was obtained in the same manner as 1. The synthesis was different by the ratio of the used reagents (copper(II) salt to the Schiff base H_3L^1). In the case of 1, it was 1:1 and in the case of 2,

it was 2:1, respectively. The amount of used substance was as follows: 0.8 mmol (0.1596 g) of copper(II) acetate monohydrate and 0.4 mmol (0.2065 g) of H_3L^1 . Deep green colored crystals 2 resulted from the slow evaporation of the solution at low temperature ($\sim 6^\circ C$).

Yield 52%; *Anal.* (%) for $C_{23}H_{32}Br_2Cu_2N_2O_{11}$ (MW: 799.40). Calcd: C, 34.53; H, 4.00; N, 3.50; Cu, 15.88. Found: C, 34.20; H, 4.30; N, 3.30; Cu, 16.10.

2.3.5. Synthesis of $[Cu_4(L^2)_2(OAc)_2] \cdot 4MeOH$ (3)

The synthesis of complex 3 was also performed in a methanol solution. The ratio of the copper(II) acetate monohydrate to the Schiff base H_3L^2 was 1:1. To a hot solution of the Schiff base (1 mmol, 0.3444 g), the stoichiometric amount of the copper(II) acetate monohydrate (1 mmol, 0.1997 g) was added. The reaction mixture was refluxed for 1 h. The green solution was left at room temperature ($20^\circ C$) for evaporation of the excess solvent. After a few days, green crystals started to form in the reaction mixture.

Yield, 43%; *Anal.* (%) for $Cu_4C_{46}H_{60}N_4O_{14}$ (MW 1147). Calcd C 48.16, H 5.27, N 4.88, Cu 22.16; found C 48.40, H 5.30, N 4.70; Cu 22.00.

2.3.6. Synthesis of $[Cu_4(L^2)_2(OAc)_2] \cdot 4H_2O \cdot 4MeOH$ (4)

The synthesis of complex 4 was carried out under similar conditions as complex 3 with the difference in the stoichiometric ratio of the copper(II) ions to the Schiff base H_3L^2 (2:1). The Schiff base was also dissolved in methanol at $55^\circ C$ and then the solution of the copper(II) acetate was added dropwise. After one hour of heating, the mixture was cooled and left at room temperature to evaporate the solvent. Dark, green crystals formed after a few days.

Yield, 66%; *Anal.* (%) for $Cu_4C_{48}H_{68}N_4O_{18}$ (MW 1219.20). Calcd C 45.31, H 5.62, N 4.60, Cu 20.85; Found C 45.20, H 5.70; N 4.30; Cu 21.00

2.4. X-ray Crystal Structure Determination

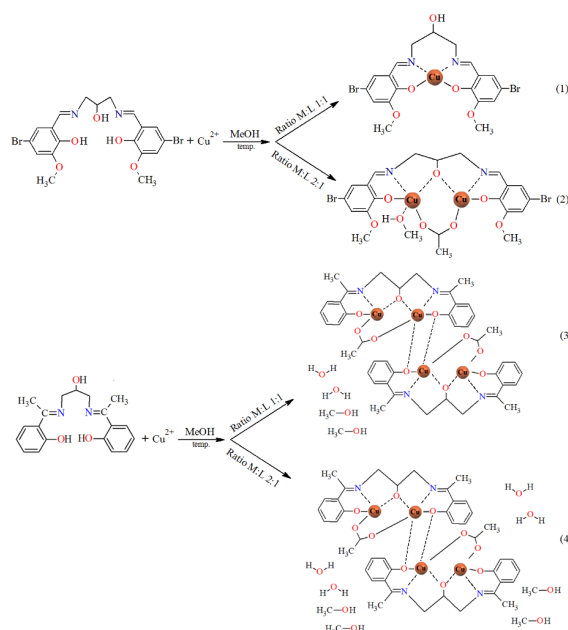
Data collections of complexes (1–4) were performed on an Oxford Diffraction Xcalibur CCD diffractometer (programs CrysAlis CCD [33]) by using graphite-monochromated $MoK\alpha$ ($\lambda = 0.71073 \text{ \AA}$). Datasets were collected at 100 K or 293 K using the ω scan technique, with an angular scan width of 1.0° . CrysAlis Red [33] was used for cell refinement and data reduction. All the data were corrected for Lorentz and polarization effects. The structures were solved by direct methods using the SHELXS-2018 program and refined on F^2 by full-matrix least-squares methods using SHELXL-2018 [34] (both implemented in the WinGX software package [35]). The carbon atom (C(10)) linked to hydroxyl oxygen atom (protonated or deprotonated) (for complexes 1, 2 and 4) and atom C(9) (for 1) exhibited disorder and were modeled over two sites with occupancies of 0.343/0.657 (1), 0.435/0.565 (2) and 0.808/0.192 (4). Additionally, in the case of 1, the distances of O(10A)–C(11), O(3)–C(10A), and O(3)–C(10B) were restrained using the DFIX command. All C-bound H atoms were placed at calculated positions and refined using a riding model with $U_{is}O(H) = 1.2$ or $1.5 U_{eq}(C)$. The water-hydrogen atoms for complexes 1 and 4 (H3W and H4W) were located on the Fourier map and refined using the DFIX command with a fixed O–H distance of $0.84/0.87 \text{ \AA}$. Next, when water hydrogen atoms with appropriate position were determined, the DFIX commands were removed and the hydrogen atoms were refined again using the AFIX 3 command with an appointed temperature factor data of -1.5000 . The water hydrogen atoms for complexes 2 and 4 (two other hydrogens H1W and H2W) were positioned geometrically and refined using a riding model (AFIX 6). The OH groups were idealized and refined using rigid groups allowed to rotate about the O–H bond (AFIX 147). A summary of crystal data, experimental details, and refinement results is provided in Table 1. The molecular plots were drawn with ORTEP3 for Windows [35] and Mercury [36] The PLATON program was used to perform the geometrical calculations [37] The CIF file refinement can be retrieved from the Cambridge Crystallographic Data Center (CCDC).

Table 1. Crystal data and structure refinement for complexes 1–4.

| Compound | 1 | 2 | 3 | 4 |
|--|------------------------------|------------------------------|------------------------------|------------------------------|
| CCDC | 2039095 | 2039094 | 2039096 | 2039097 |
| Temperature K | 100 (2) | 100 (2) | 100 (2) | 293 (2) |
| Crystal system | triclinic | triclinic | monoclinic | monoclinic |
| Space group | $P\bar{1}$ | $P\bar{1}$ | $P2_1/n$ | $P2_1/c$ |
| a (Å) | 9.7268 (5) | 11.0947 (4) | 12.3661 (4) | 11.4074 (3) |
| b (Å) | 9.9259 (5) | 11.3975 (5) | 15.4875 (4) | 15.4271 (4) |
| c (Å) | 11.5160 (6) | 12.1621 (4) | 13.6765 (4) | 14.2363 (3) |
| α (°) | 92.895 (4) | 92.688 (3) | 90.00 | 90.00 |
| β (°) | 108.791 (5) | 106.584 (3) | 116.231 (4) | 92.094 (2) |
| γ (°) | 98.226 (4) | 104.224 (4) | 90.00 | 90.00 |
| Volume (Å ³) | 1036.2 (1) | 1417.4 (1) | 2349.6 (1) | 2503.67 (11) |
| Z | 2 | 2 | 2 | 2 |
| Calculated density (g cm ⁻³) | 1.909 | 1.873 | 1.621 | 1.617 |
| μ (mm ⁻¹) | 4.950 | 4.380 | 1.857 | 1.754 |
| Absorption correction | multi-scan | multi-scan | multi-scan | multi-scan |
| F(000) | 590 | 800 | 1184 | 1264 |
| Crystal size (mm) | 0.60 × 0.30 × 0.20 | 0.20 × 0.10 × 0.05 | 0.45 × 0.25 × 0.20 | 0.35 × 0.35 × 0.20 |
| θ range (°) | 2.66 to 27.10 | 2.72 to 27.10 | 2.63 to 26.37 | 2.61 to 26.37 |
| Reflections collected/unique | 7749/4571 | 10884/6261 | 16637/4764 | 10392/4993 |
| R _i /N _t | 0.0271 | 0.0340 | 0.0319 | 0.0326 |
| Data/restraints/parameters | 4571/3/293 | 6261/0/381 | 4764/0/314 | 4993/0/360 |
| Goof on F ² | 1.095 | 1.048 | 1.057 | 1.083 |
| Final R indices[I > 2 σ (I)] | R1 = 0.0448, wR2 = 0.0999 | R1 = 0.0409, wR2 = 0.0958 | R1 = 0.0316, wR2 = 0.0789 | R1 = 0.0352, wR2 = 0.0850 |
| R indices(all data) | R1 = 0.0584, wR2 = 0.1075 | R1 = 0.0547, wR2 = 0.1054 | R1 = 0.0410, wR2 = 0.0842 | R1 = 0.0452, wR2 = 0.0919 |
| Largest diff. peak/hole, e Å ⁻³ | 1.144/−1.012 | 1.853/−0.558 | 1.143/−0.387 | 0.811/−0.419 |

3. Results

The reaction of copper(II) acetate and Schiff bases gives rise to mono-, di-, or tetranuclear derivatives, depending on the reaction conditions: ratio of reagents and the nature of the substituent in the benzene ring of the N,O-donor ligands. The results are summarized in Scheme 4.



Scheme 4. The route to the synthesis of 1–4 (for complex 1 and 2, the solvent molecules in the outer coordination sphere were omitted).

3.1. Fourier Transform Infrared (FTIR) Spectra

The used Schiff bases: 2,2'-(2-hydroxypropane-1,3-diyl)bis[nitrilomethylidene]]bis(4-bromo-6-methoxyphenol) H_3L^1 and H_3L^2 , respectively, are potentially capable of forming coordinate bonds with various metal ions through the azomethine, phenolic, hydroxyl, or methoxy groups. The FTIR spectra of the Cu(II) coordination compounds 1–4 were compared with the spectra of H_3L^1 and H_3L^2 (Figures 1 and 2, Figures S1–S6) in order to obtain information about the binding mode of the Schiff base ligands to copper(II) ions. The position and/or the intensities of the peaks are expected to be changed upon complexation.

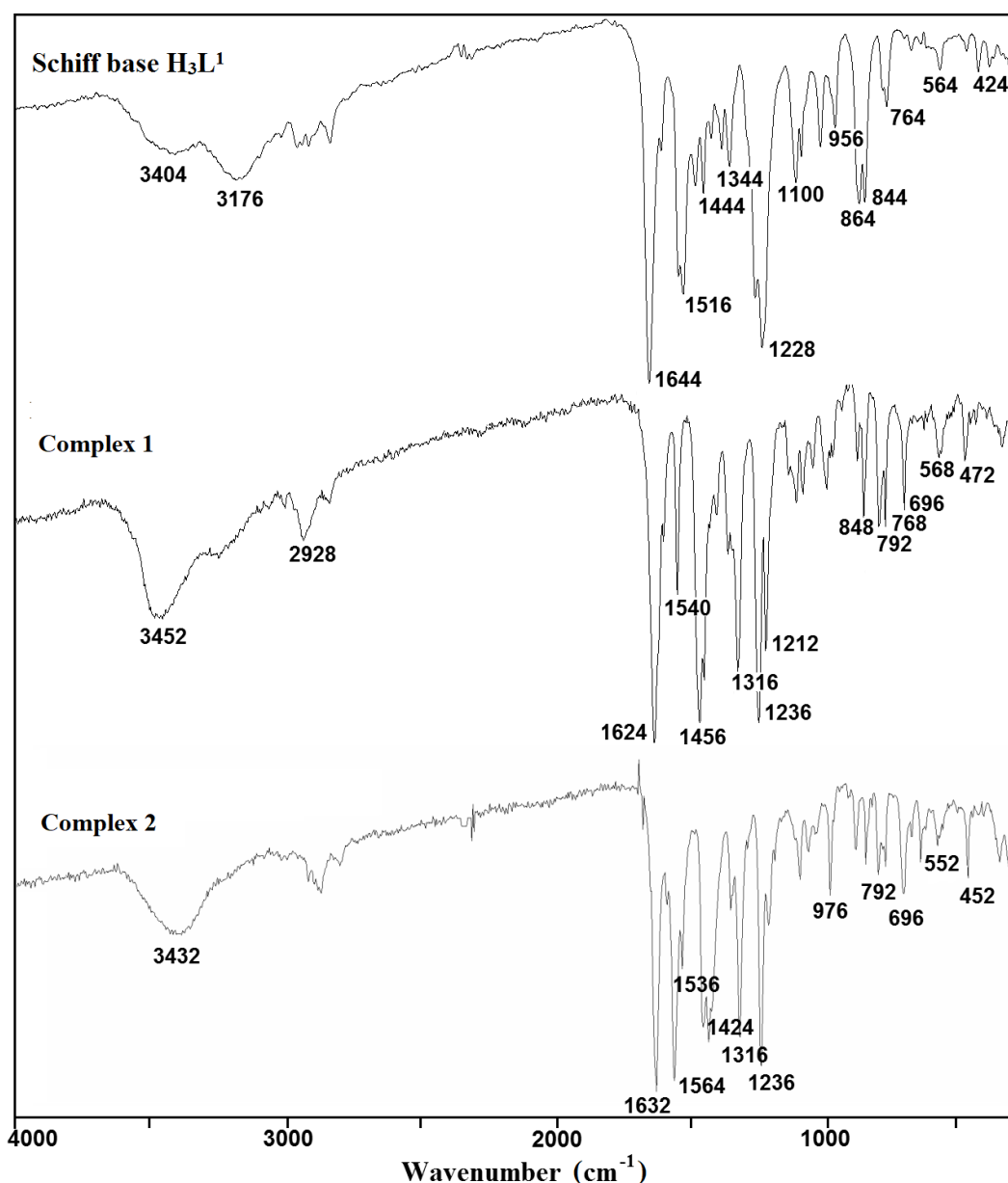


Figure 1. Fourier transform infrared (FTIR) spectra of the Schiff base ligand H_3L^1 and complexes 1 and 2.

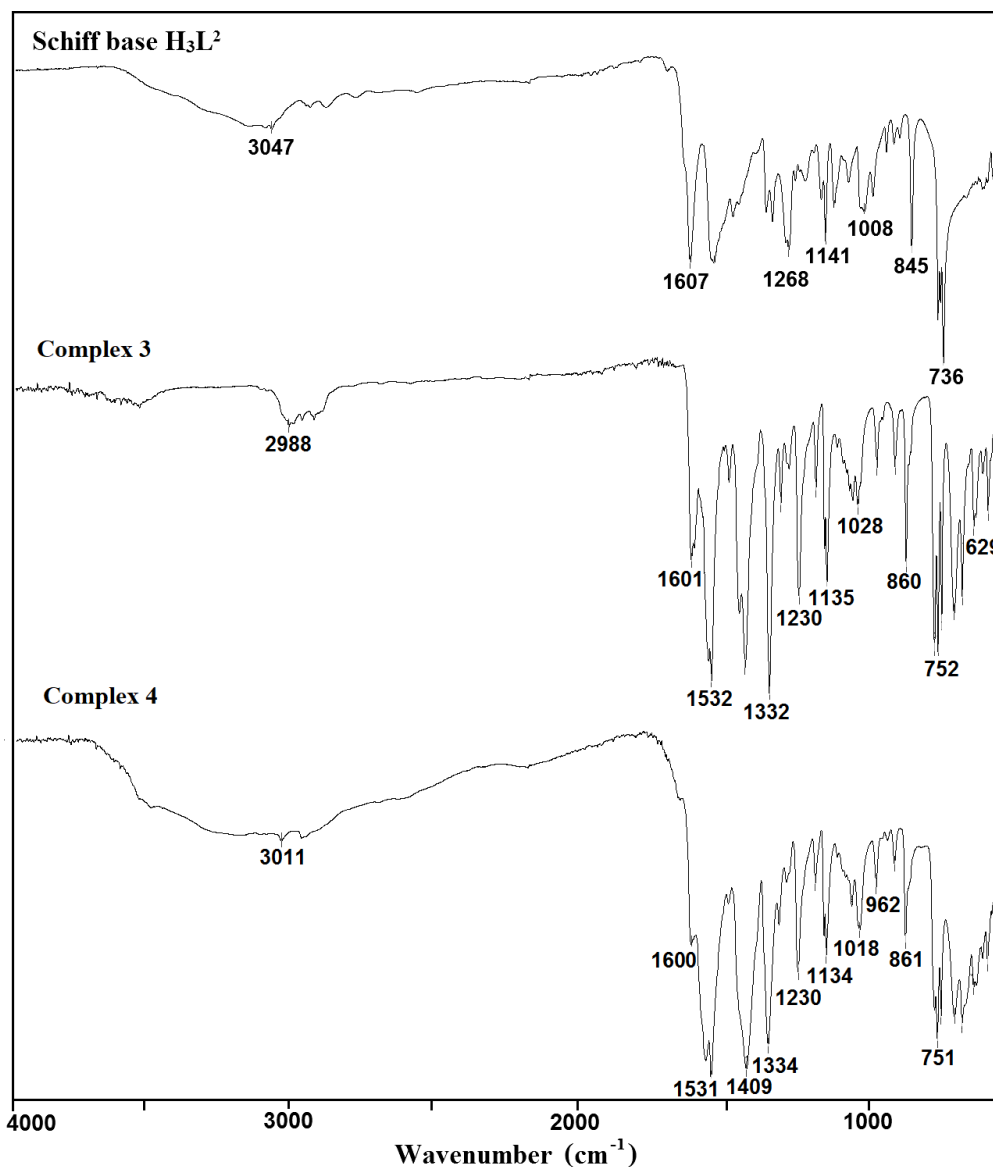


Figure 2. FTIR spectra of the Schiff base ligand H₃L² and complexes 3 and 4.

In the spectra of the free ligands H₃L¹ and H₃L², strong sharp absorption bands present at around 1644 and 1607 cm⁻¹, respectively, can be assigned for the imine stretching frequency $\nu(\text{C}=\text{N})$. Upon complexation of H₃L¹, this band is redshifted to 1624 (1) and 1632 cm⁻¹ (2). A similar downward shift was observed in the peak positions of $\nu(\text{C}=\text{N})$ stretch vibrations of 3 (1601 cm⁻¹) and 4 (1600 cm⁻¹) having in the crystal structure deprotonated H₃L² as a ligand (1607 cm⁻¹). This feature may be explained by the withdrawing of electrons from nitrogen to Cu(II) ions due to the coordination. The strong phenolic stretching vibration $\nu(\text{C}-\text{O})$ at 1236 (1 and 2) and 1230 cm⁻¹ (3 and 4) confirmed that oxygen atoms coordinate to metal ions. A medium or weak broad band with a maximum at around 3452 (1), 3432 (2), 3490 (3), and 3180 cm⁻¹ (4) can be assigned to the OH stretching vibrations, $\nu(\text{O}-\text{H})$ of OH groups with different chemical environments (i.e., water/methanol molecules and/or hydroxyl groups of the Schiff base ligand that remain protonated in compound 1, as confirmed by X-ray analysis). In the FTIR spectra of complexes 2–4, the strong bands characteristic of asymmetric $\nu_{\text{as}}(\text{OCO})$ and symmetric $\nu_{\text{s}}(\text{OCO})$ stretching vibrations of the carboxylate group were observed at 1564 and 1424 (2), 1532 and 1417 (3), and 1531 and 1409 cm⁻¹ (4), respectively [38–40]. The differences between values of asymmetric $\nu_{\text{as}}(\text{OCO})$ and symmetric $\nu_{\text{s}}(\text{OCO})$ stretching vibrations (115–140 cm⁻¹) of a bridging carboxylate group of the acetic ion corresponded with those reported in the literature [32,41].

3.2. Description of the Molecular Structure

The results of X-ray analysis are presented in Figures 3–10, Figures S7 and S8. The selected bond distances and bond angles are given in Table 2. The hydrogen bond parameters are listed in Table S2 (Supplementary Materials).

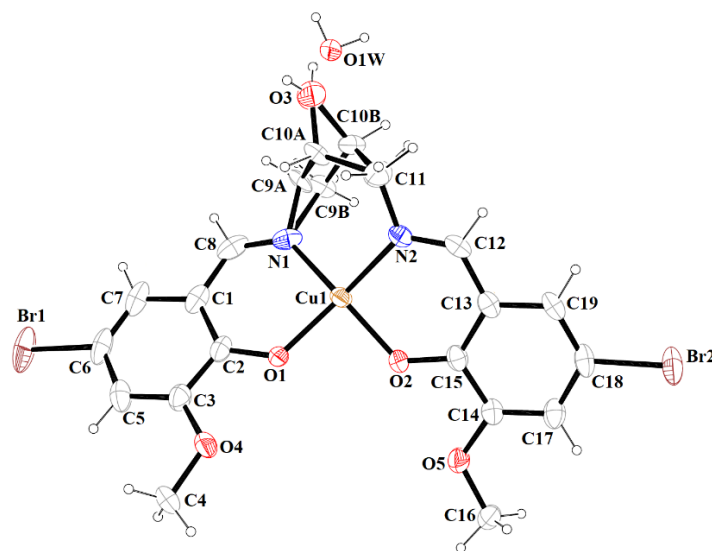


Figure 3. A view of 1 with the atom numbering scheme. Displacement ellipsoids are drawn at the 60% probability level.

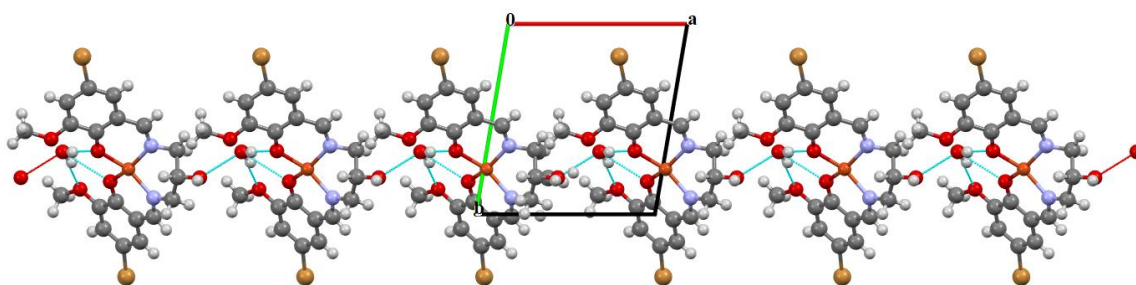


Figure 4. Part of the crystal structure of complex 1 showing O–H...O hydrogen bonds and formation of the 1D chain along the *a* direction.

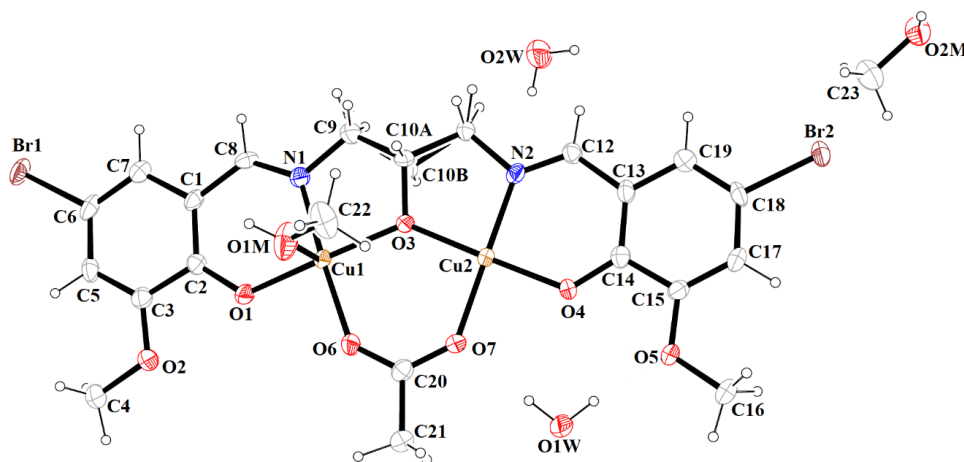


Figure 5. Molecular structure and numbering atoms scheme of 2. Displacement ellipsoids are drawn at the 60% probability level.

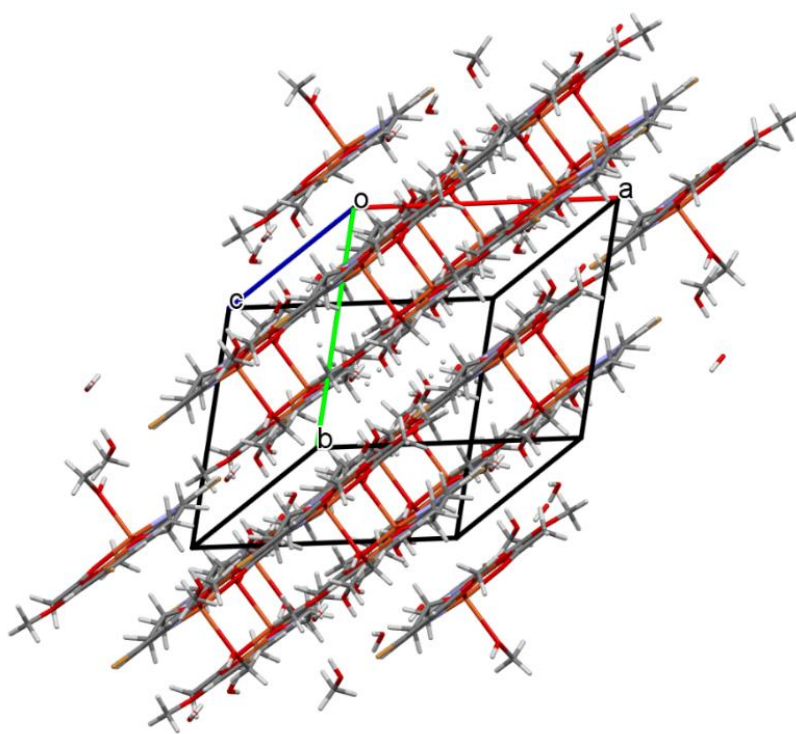


Figure 6. Packing of complex 2 (the hydrogen bonds were omitted for the sake of clarity).

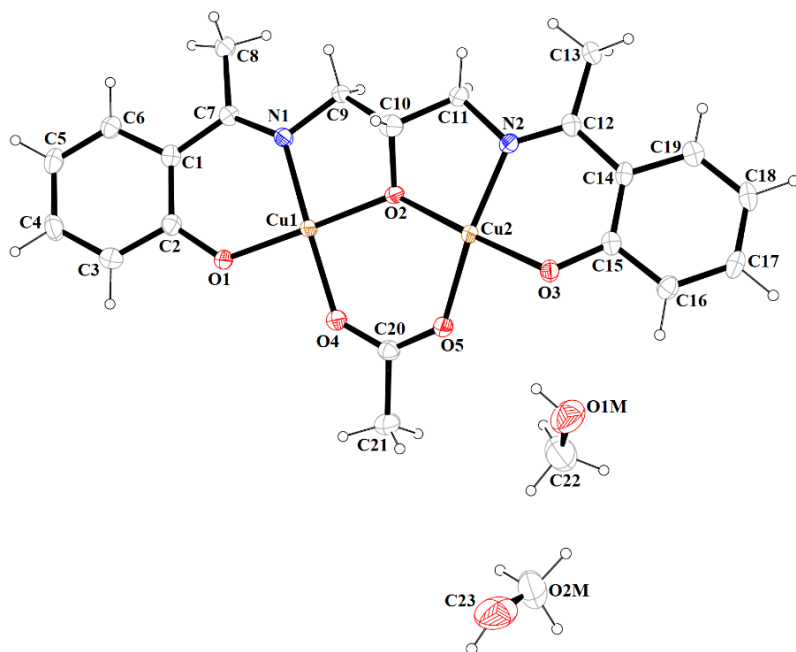


Figure 7. A view of asymmetric unit of 3, showing the atom-numbering scheme. Displacement ellipsoids are drawn at the 60% probability level.

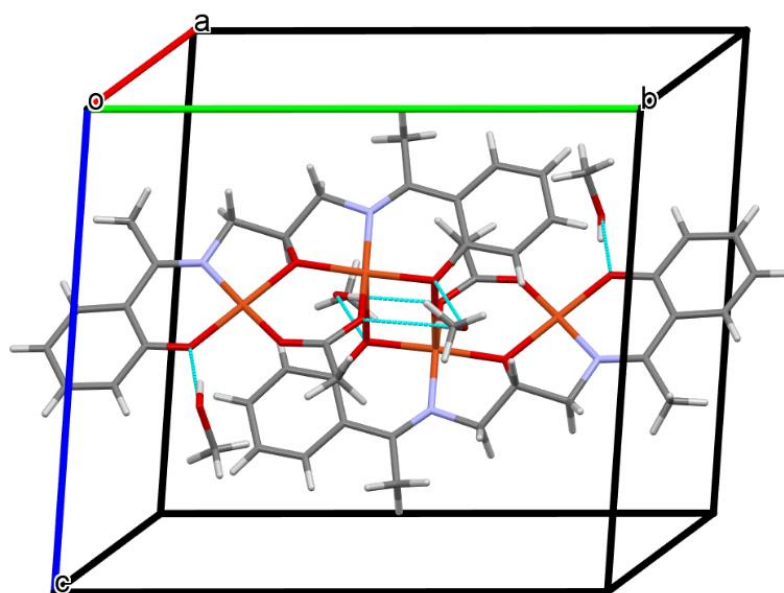


Figure 8. A view of O–H...O hydrogen bonds in a tetranuclear unit of 3.

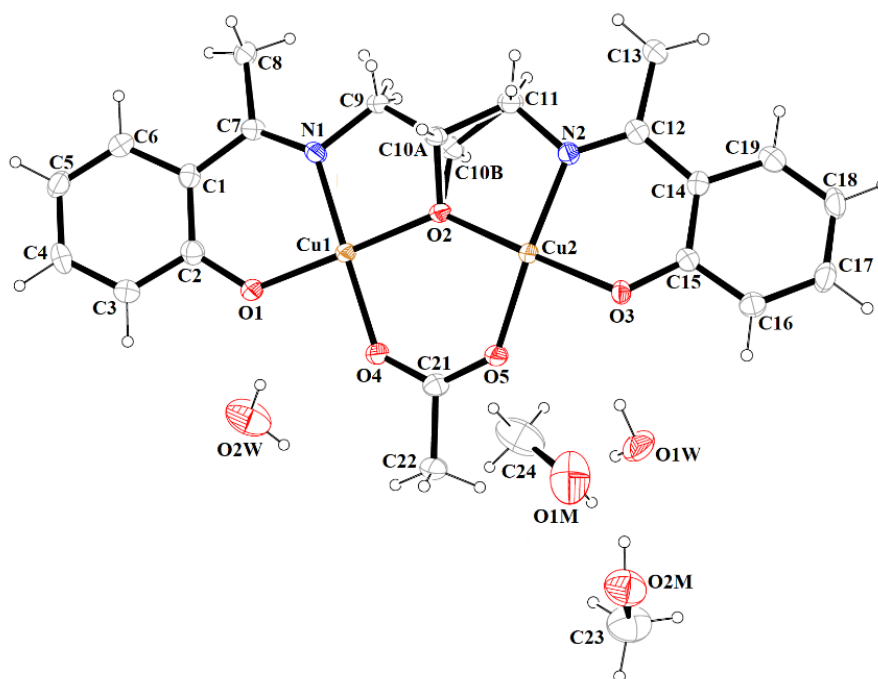


Figure 9. A view of asymmetric unit of 4, showing the atom-numbering scheme. Displacement ellipsoids are drawn at the 60% probability level.

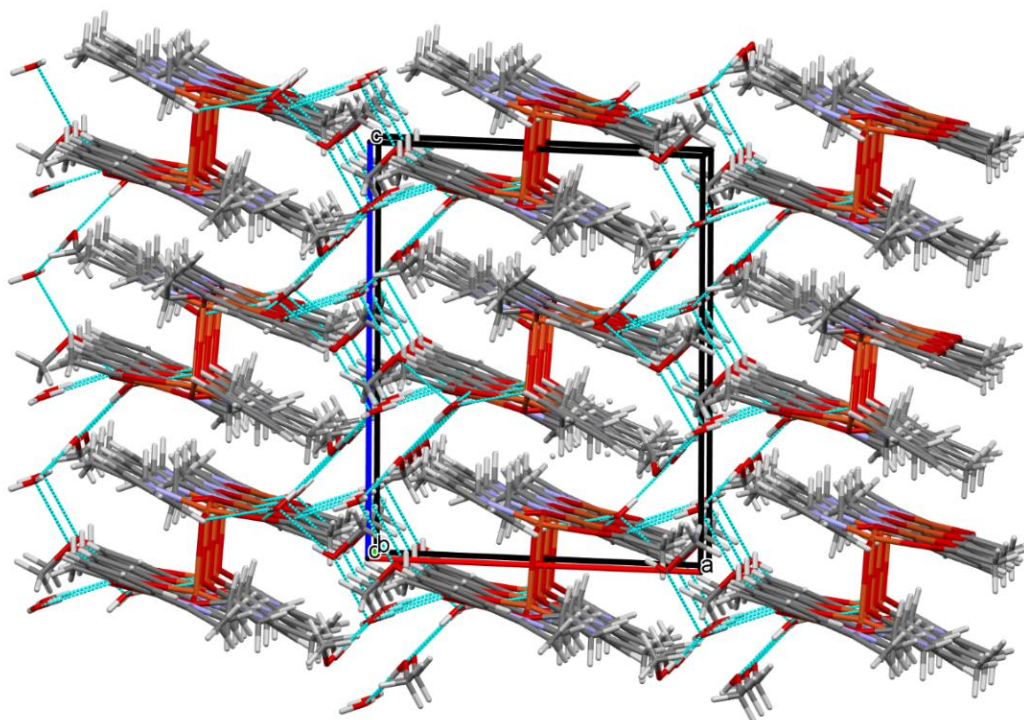


Figure 10. Part of the crystal structure of complex 4 showing the O–H...O hydrogen bonds and the formation of a three-dimensional supramolecular network.

Table 2. Selected geometric parameters for the copper(II) complexes 1–4.

| 1 | | | |
|-------------------------|-------------|------------------|-------------|
| <i>Bond lengths (Å)</i> | | | |
| Cu(1)–N(1) | 1.951 (3) | Cu(1)–O(1) | 1.912 (2) |
| Cu(1)–N(2) | 1.955 (3) | Cu(1)–O(4) | 1.910 (3) |
| <i>Angle (°)</i> | | | |
| O(4)–Cu(1)–O(1) | 88.80 (11) | N(1)–Cu(1)–N(2) | 94.37 (14) |
| O(4)–Cu(1)–N(1) | 156.13 (12) | O(4)–Cu(1)–N(2) | 93.45 (12) |
| O(1)–Cu(1)–N(1) | 92.83 (13) | O(1)–Cu(1)–N(2) | 156.70 (12) |
| 2 | | | |
| <i>Bond lengths (Å)</i> | | | |
| Cu(1)–N(1) | 1.946 (3) | Cu(2)–O(3) | 1.905 (2) |
| Cu(1)–O(1) | 1.918 (2) | Cu(2)–N(2) | 1.925 (3) |
| Cu(1)–O(3) | 1.934 (2) | Cu(2)–O(4) | 1.895 (2) |
| Cu(1)–O(6) | 1.965 (3) | Cu(2)–O(7) | 1.952 (3) |
| Cu(1)–O(1M) | 2.321 (3) | | |
| <i>Angles (°)</i> | | | |
| O(1)–Cu(1)–O(3) | 168.39 (12) | N(1)–Cu(1)–O(1M) | 94.32 (13) |
| O(1)–Cu(1)–N(1) | 93.04 (11) | O(6)–Cu(1)–O(1M) | 92.78 (12) |
| O(3)–Cu(1)–N(1) | 84.24 (11) | O(4)–Cu(2)–O(3) | 178.70 (11) |
| O(1)–Cu(1)–O(6) | 87.53 (10) | O(4)–Cu(2)–N(2) | 93.33 (11) |
| O(3)–Cu(1)–O(6) | 93.79 (10) | O(3)–Cu(2)–N(2) | 85.39 (11) |
| N(1)–Cu(1)–O(6) | 172.86 (12) | O(4)–Cu(2)–O(7) | 86.81 (11) |
| O(1)–Cu(1)–O(1M) | 91.84 (11) | O(3)–Cu(2)–O(7) | 94.48 (11) |
| O(3)–Cu(1)–O(1M) | 99.61 (11) | N(2)–Cu(2)–O(7) | 177.03 (13) |

Table 2. Cont.

| 3 | | | |
|-------------------------|------------|-------------------------------|------------|
| <i>Bond lengths (Å)</i> | | | |
| Cu(1)–O(1) | 1.882 (2) | Cu(2)–O(2) | 1.911 (2) |
| Cu(1)–O(2) | 1.905 (2) | Cu(2)–O(3) | 1.898 (2) |
| Cu(1)–O(4) | 1.951 (2) | Cu(2)–O(5) | 1.991 (2) |
| Cu(1)–N(1) | 1.955 (2) | Cu(2)–N(2) | 1.970 (2) |
| | | Cu(2)–O(3) ^{3a} | 2.399 (2) |
| <i>Angles (°)</i> | | | |
| O(1)–Cu(1)–O(2) | 178.33 (7) | O(2)–Cu(2)–N(2) | 84.89 (8) |
| O(1)–Cu(1)–O(4) | 87.32 (8) | O(3)–Cu(2)–O(5) | 87.87 (7) |
| O(2)–Cu(1)–O(4) | 93.96 (7) | O(2)–Cu(2)–O(5) | 94.31 (7) |
| O(1)–Cu(1)–N(1) | 93.15 (8) | N(2)–Cu(2)–O(5) | 162.05 (8) |
| O(2)–Cu(1)–N(1) | 85.69 (8) | O(3)–Cu(2)–O(3) ^{3a} | 85.82 (7) |
| O(4)–Cu(1)–N(1) | 174.11 (8) | O(2)–Cu(2)–O(3) ^{3a} | 95.48 (7) |
| O(3)–Cu(2)–O(2) | 177.47 (7) | N(2)–Cu(2)–O(3) ^{3a} | 108.34 (7) |
| O(3)–Cu(2)–N(2) | 92.63 (8) | O(5)–Cu(2)–O(3) ^{3a} | 89.60 (7) |
| 4 | | | |
| <i>Bond lengths (Å)</i> | | | |
| Cu(1)–O(1) | 1.883(2) | Cu(2)–O(2) | 1.907(2) |
| Cu(1)–O(2) | 1.902(2) | Cu(2)–O(3) | 1.903(2) |
| Cu(1)–O(4) | 1.943(2) | Cu(2)–O(5) | 1.952(2) |
| Cu(1)–N(1) | 1.952(2) | Cu(2)–N(2) | 1.955(2) |
| | | Cu(2)–O(3) ^{4a} | 2.485(2) |
| <i>Angles (°)</i> | | | |
| O(1)–Cu(1)–O(2) | 178.67(8) | O(2)–Cu(2)–O(5) | 94.36(8) |
| O(1)–Cu(1)–O(4) | 86.64(8) | O(3)–Cu(2)–N(2) | 93.08(9) |
| O(2)–Cu(1)–O(4) | 94.69(8) | O(2)–Cu(2)–N(2) | 85.13(9) |
| O(1)–Cu(1)–N(1) | 93.42(9) | O(5)–Cu(2)–N(2) | 166.83(8) |
| O(2)–Cu(1)–N(1) | 85.26(9) | O(2)–Cu(2)–O(3) ^{4a} | 95.48(7) |
| O(4)–Cu(1)–N(1) | 176.48(8) | O(3)–Cu(2)–O(3) ^{4a} | 86.13(7) |
| O(3)–Cu(2)–O(2) | 177.87(8) | O(5)–Cu(2)–O(3) ^{4a} | 86.60(7) |
| O(3)–Cu(2)–O(5) | 87.13(8) | N(2)–Cu(2)–O(3) ^{4a} | 106.56(7) |

Symmetry codes: (3a) $-x + 1, -y + 1, -z + 1$; (4a) $-x + 1, -y, -z$.

The mononuclear complex $[\text{Cu}(\text{HL}^1)] \cdot \text{H}_2\text{O}$ (1) crystallizes in the centrosymmetric triclinic system, space group $P-1$. The doubly deprotonated Schiff base $(\text{HL}^1)^{2-}$ acts as a tetradentate ligand and the Cu^{II} is coordinated by a pair of phenolate oxygen (O(1) and O(4)) and imine nitrogen (N(1) and N(2)) atoms (Figure 3). The alcohol group of the aliphatic chain of the Schiff base ligand remains protonated and acts as a hydrogen bond donor to a molecule of water. The water molecule further acts as a hydrogen bond donor, interacting with two phenolate and one methoxy oxygen atoms of the Schiff base ligand (Table S2). Consequently, this results in the formation of the hydrogen bonded chain that propagates parallel to the crystallographic a -axis (Figure 4). The central atom has distorted square planar coordination with a significant tetrahedral distortion as indicated by the less than linear bond angles ($156.13(12)^\circ$ O(4)–Cu(1)–N(1) and $156.70(12)^\circ$ O(1)–Cu(1)–N(2)) and the dihedral angle between the two N–Cu(1)–O planes ($\theta = 32.42^\circ$). This can be confirmed by the structural index parameters τ_4 [42] and τ_4' [43], which were equal to 0.33. The Cu–O and Cu–N bonds were within normal values and comparable to those observed in the related copper(II) complexes (Table S1).

In contrast to 1, complex 2 crystallizes in the triclinic system, space group $P-1$ as a binuclear unit $[\text{Cu}_2(\text{L}^1)(\text{OAc})\text{MeOH}] \cdot 2\text{H}_2\text{O} \cdot \text{MeOH}$ (Figure 5). In its crystal structure, the metal centers Cu(1) and Cu(2) are double bridged by the oxygen atoms of the alkoxide group and the carboxylate group of the acetate ion, respectively. Compound 2 crystallizes with two methanol and two water molecules, one methanol molecule is axially coordinated to one copper atom Cu(1) (Cu(1)–O(1M) = 2.322(3) Å), leading to almost ideal square pyramidal geometries (formed by O(2), O(3), O(6), O(1M), and N(1) atoms), which was confirmed by the value of the τ_5 parameter (0.03) [44]. In the case of the Cu(2) center, the NO_3 atoms showed less tetrahedral distortion from the square planar geometry than that observed for N_2O_2 core around the Cu^{II} center in complex 1, as indicated by the structural index

parameters ($\tau_4 = 0.13$ and $\tau_4' = 0.12$). The presence of O–H...O and C–H...O bonds (Table S2) expanded the structure of complex 2 into the 3D network presented in Figure 6.

Complex 3 crystallizes in the centrosymmetric monoclinic space group $P2_1/n$. Single-crystal X-ray analysis showed that the asymmetric unit of 3 contains two crystallographically independent Cu(II) centers, one deprotonated Schiff base ($(L^2)^{3-}$), the acetate ion, and two methanol molecules (Figure 7). Both Cu^{II} ions are coordinated by one phenoxy, alkoxy, and carboxylate oxygen and imine nitrogen atoms. Additionally, the Cu(2) ion is bound by the phenolate oxygen of second $(L^2)^{3-}$ ions, which leads to the formation of a tetranuclear complex. The Cu(1) atom resides in an almost perfect square planar environment that was confirmed by the values of the τ_4 and τ_4' parameters [42,43], which were equal to 0.05 and 0.04, respectively. In contrast to complex 2, the coordination polyhedron around the Cu(2) ion was a significant distorted square pyramid ($\tau_5 = 0.26$) [44]. The Cu–O and Cu–N bonds were within the normal values and were comparable to those observed in the related copper(II) complexes [3,32,45]. The dimeric units $[Cu_4(L^2)_2(OAc)_2]$ and methanol molecules were consolidated by the O–H...O hydrogen bonds (Figure 8). The presence of weak C–H...O interactions connects the discrete units into a layered structure (Figure S8).

Complex 4 crystallizes in the monoclinic crystal system in space group $P2_1/c$ with the asymmetric unit shown in Figure 9. Similar to complex 3, the asymmetric dimeric units are linked through the phenoxo oxygen atom of the Schiff base. The coordination environments around metal centers are also similar to those observed for complex 3. In complex 4, the structural index parameters τ_4 and τ_4' were equal to 0.03, indicating less significant tetrahedral distortion from the square planar geometry than observed for 3. The coordination polyhedrons around Cu(2) ions had a distorted square pyramidal geometry that was confirmed by the value of τ_5 parameter (0.18). The structure of complex 4 also differed from 3 in the number and type of solvent molecules (i.e., it contains four additional water molecules). The presence of methanol and water molecules cause the stabilization of a structure by the formation of O–H...O hydrogen bonds and consolidates tetranuclear units into a three-dimensional supramolecular network (Figure 10).

3.3. Thermal Analysis

The thermal properties of complexes 1–4 were studied in an air atmosphere and the thermogravimetric (TG), the differential thermal analysis (DTG) and the differential scanning calorimetric (DSC) curves and TG-FTIR spectra are presented in Figures 11–16, Figures S9 and S10.

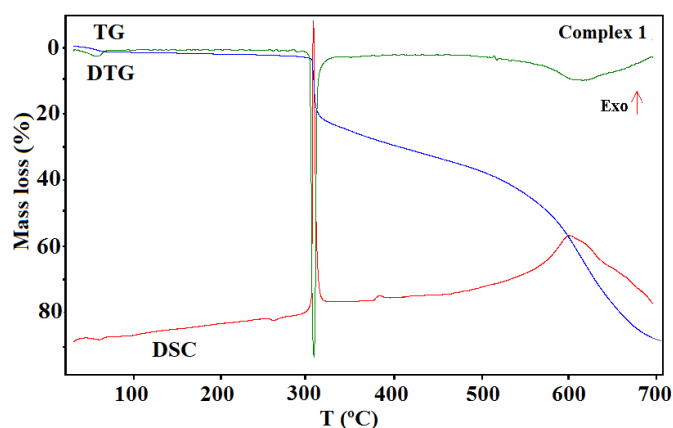


Figure 11. The thermogravimetric (TG), the differential thermal analysis (DTG), and the differential scanning calorimetric (DSC) curves of the thermal decomposition of complex 1 in air.

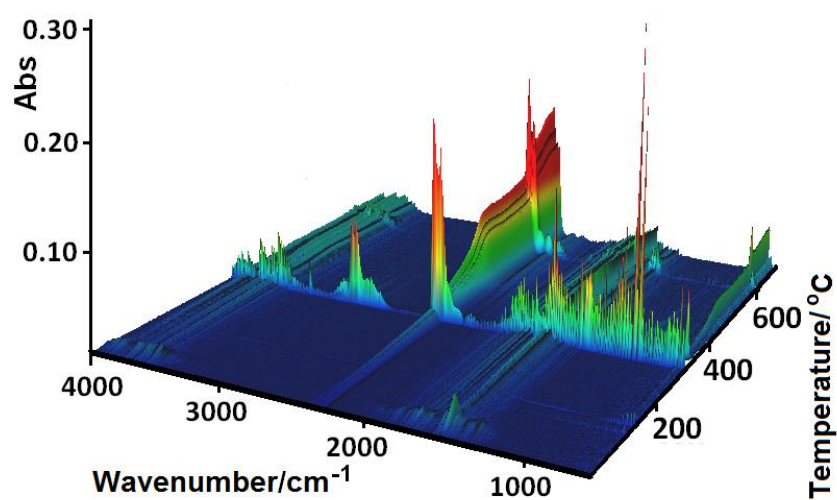


Figure 12. FTIR spectra of the gaseous products evolved during the decomposition process of 1.

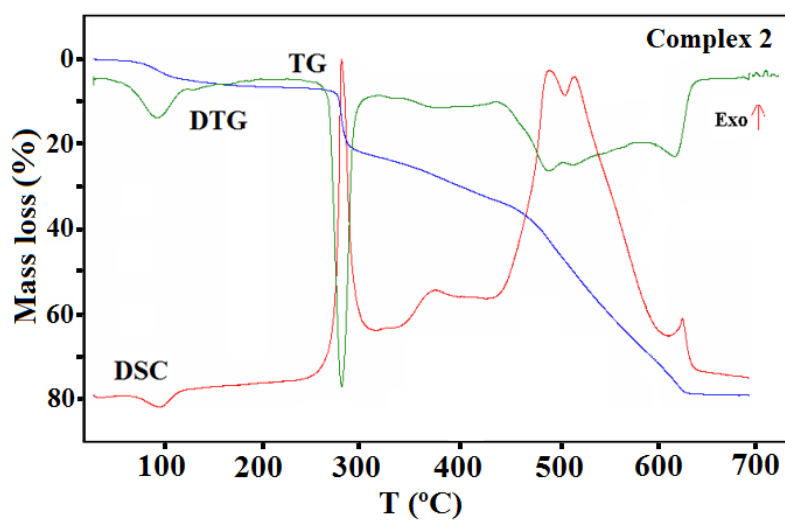


Figure 13. TG, DTG, and DCS curves of thermal decomposition of complex 2 in air.

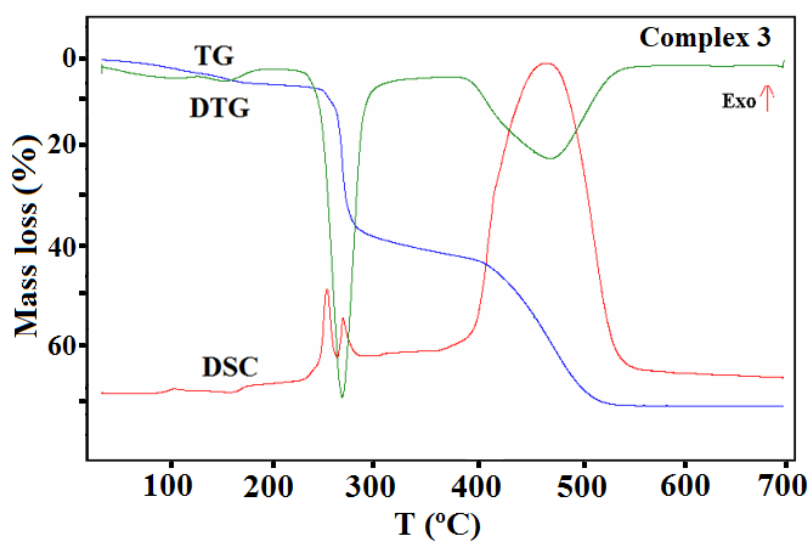


Figure 14. TG, DTG, and DCS curves of thermal decomposition of complex 3 in air.

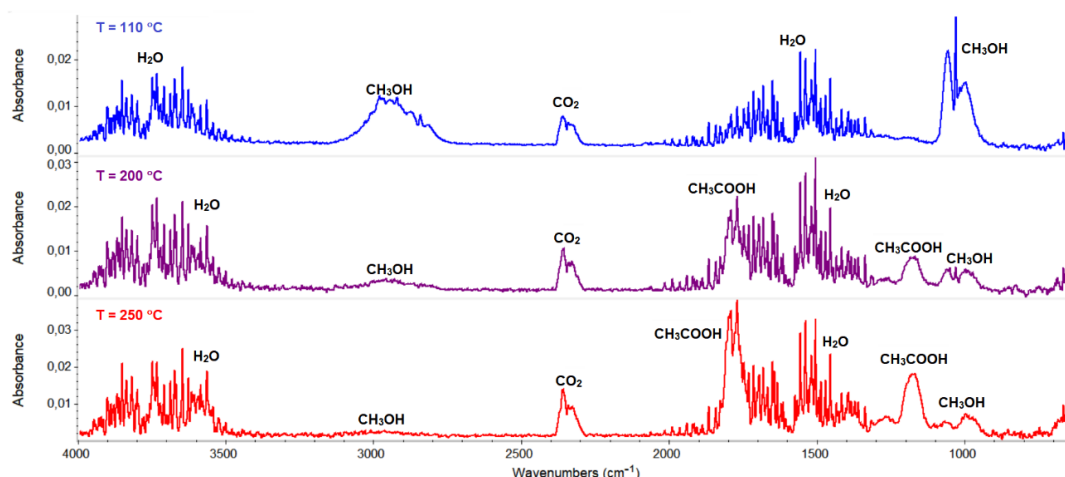


Figure 15. FTIR spectra of gaseous products evolved during the decomposition process of 3.

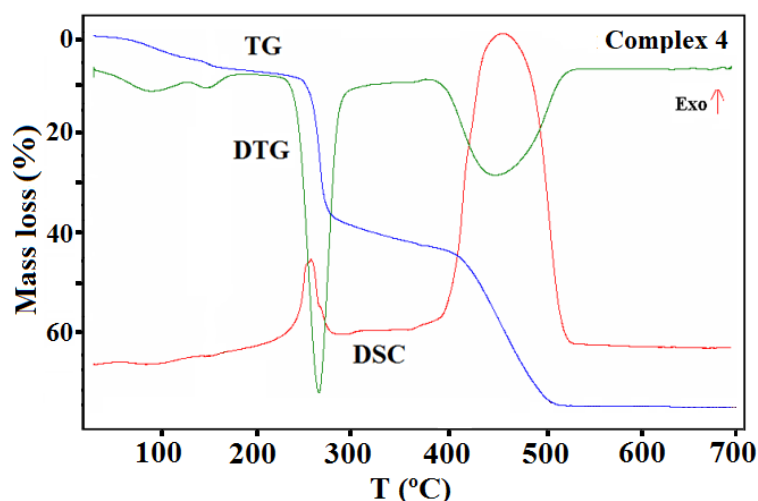


Figure 16. TG, DTG, and DSC curves of the thermal decomposition of complex 4 in air.

The shape of the TG curves indicates that 1–4 are stable at room temperature. In 1 (Figure 11), the initial decomposition step seen in the range of 45–70 °C (centered at ca. 59 °C) concerns the release of one water molecule with a mass loss of 2.60% (calcd. 3.02%). This step is accompanied by the small endothermic effect recorded on the DSC curve related to the dehydration process. The obtained product is stable until ca. 290 °C, and then decomposes until stabilization at a temperature about 700 °C. In the DSC plot, two exothermic processes were detected. The final product mass loss was 13.40% for the initial compound 1 sample, being consistent with CuO (calcd. 13.35%). Similar mass losses were found on the TG curve recorded under nitrogen. The FTIR spectra of the emitted gases confirmed that during this stage, molecules of water were removed from the structure of 1. The main gaseous products resulting from thermal degradation of 1 were mainly: H₂O, CO₂, CO, and NH₃ (Figure 12).

The TG, DTG, and DSC curves of compound 2 are shown in Figure 13. The first step recorded on the TG curve in the temperature range of 70–110 °C (centered at ca. 97 °C) was related to the dehydration process and concerned the release of two water molecules with a mass loss of 4.90% (calcd. 4.50%).

This step was also accompanied by an endothermic effect. The rapid mass loss of 15.00% at 270 °C can be accounted for by the loss of the methanol molecules and the acetic acid (calcd. 15.40%). The next step of the decomposition occurred in the range of 320–630 °C and can be due to the Schiff base ligand decomposition. The final product mass was 19.80%, which is comparable to the calculated value of

19.90% for CuO. The TG-FTIR of the gaseous product released during thermal analysis under an inert atmosphere is presented in Figure S9.

In the case of complex 3 (Figure 14), the mass changes on the TG curve at a temperature up to 185 °C can be assigned to the desolvation processes. During this stage, two methanol molecules are gradually removed from the structure (calcd. mass loss 5.58%, found 6.32%). The remaining solvent molecules are lost in the next step together with the acetate ions. This step also relates to the partial defragmentation, which results in the release of volatile fragments of the organic ligand. The formed intermediate, unstable organic matrix undergoes combustion in the last stage, which was confirmed by the large exothermic effect on the DSC curve. The final decomposition product formed at 558 °C was CuO. The found overall mass loss was 71.83% while the calculated one was 72.26%.

The thermal behavior of complex 3 was also studied in the inert atmosphere of nitrogen. The first stage was similar to that observed in air (i.e., desolvation process). In contrast to the oxidizing atmosphere, a smaller amount of solvent (one and half molecule, found mass loss 4.1%) was released. The remaining methanol molecules were removed from the complex together with the acetate ions, which was confirmed in the FTIR spectra of the gaseous products. The characteristic vibration bands of CH₃OH were observed in the wavenumber ranges between 2750–3150 and 950–1100 cm⁻¹, together with those assigned to the acetic acid and their products of the pyrolysis (i.e., CO₂ and H₂O) (Figure 15). The further heating of the sample was related to the pyrolysis of the Schiff base ligand, which led to the formation of the following gaseous products: CO₂, NH₃, H₂O, C₆H₅OH, and CO [46].

Complex 4 undergoes similar processes on heating as compound 3 (Figure 16). The desolvation process starts ca. 45 °C. In the first step, three water molecules were probably lost (calcd. mass loss 4.43%, found 4.36%). The same process was also observed on the TG curve recorded in a nitrogen atmosphere (the found initial mass loss was 4.06%).

Analysis of the FTIR spectra of the evolved gas phase confirmed that only water molecules were released during first step of the desolvation process (Figure S10). The remaining water molecule was given off in the next stage, during which the methanol was also gradually removed from the structure. At 175 °C, the mass loss found on the TG curve was 6.94%, which corresponded to a loss of four water molecules and a half molecule of methanol (calcd. mass loss 7.22% in an oxidizing and 6.85% in an inert atmosphere). The other methanol molecules were lost along with the release of the acetate ions. The acetic ions were registered in the FTIR spectra of gaseous products as acetic acid (Figure S10). During this stage, at higher temperature, the decomposition and the combustion/pyrolysis of the Schiff base was also observed. The final product of the thermal decomposition of 4 in air was CuO, which formed at 525 °C. In contrast, under nitrogen stream, the decomposition process of ligand is not finished; the residue remaining after the analysis at 700 °C was 44.40%. Pyrolysis of the Schiff base ligand was associated with the emission of gases similar to those mentioned for complex 3 as well as CH₄.

4. Conclusions

The deprotonated heptadentate and pentadentate Schiff base ligands H₃L¹ and H₃L² in all compounds coordinated Cu(II) ions through the azomethine as well as phenolate groups. The presence of an additional hydroxyl group in the structure of the Schiff bases allowed us to synthesis di- and tetranuclear complexes. In the crystal structure of polynuclear compounds, the metal ions are additionally linked via acetate ions and the alkoxy group. In 2, 3, and 4, two types of metal center were present (i.e., four- and five-coordinated). The coordination environment around the Cu^{II} centers can be described as a distorted square pyramid (C.N. = 5) or square planar (C.N. = 4).

Thermal analysis indicated that the coordination compounds 1–4 are thermally stable at room temperature. Their decomposition processes in air appear to follow a similar trend, starting from losing the crystallization solvent molecules, followed by the ligand decomposition, and finally forming CuO. In contrast to an oxidizing atmosphere, under a nitrogen atmosphere, the pyrolysis process of Schiff base ligands is not finished.

Supplementary Materials: The following are available online at <http://www.mdpi.com/2073-4352/10/11/1004/s1>, Table S1: List of chosen mono- and polynuclear Schiff base complexes of Cu^{II} found in the CSD search. Table S2: Hydrogen bonding and C–H... π interactions geometry [Å] for complexes 1–4. Figure S1: FTIR spectra of the Schiff base ligand H₃L¹ and complex 1. Figure S2: FTIR spectra of the Schiff base ligand H₃L¹ and complex 2. Figure S3: FTIR spectra of the complexes 1 and 2. Figure S4: FTIR spectra of the Schiff base ligand H₃L² and complex 3. Figure S5: FTIR spectra of the Schiff base ligand H₃L² and complex 4. Figure S6: FTIR spectra of the complexes 3 and 4. Figure S7: The packing of structure 1 along the *a* direction. Figure S8: The crystal structure packing of complex 3 showing formed layers via C–H...O interactions. Figure S9: FTIR spectra of gaseous products of complex 2, decomposition in nitrogen. Figure S10: FTIR spectra of gaseous products of complex 4 decomposition in nitrogen.

Author Contributions: Conceptualization, D.O., B.C., and A.B.; Writing—original draft preparation, D.O., B.C., and A.B.; Investigation, D.O., B.C., and A.B.; Formal analysis, D.O., B.C., and A.B.; Methodology, B.C. and A.B.; Software, A.B. All authors have read and agreed to the published version of the manuscript.

Funding: This research received no external funding.

Conflicts of Interest: The authors declare no conflict of interest.

References

1. More, M.S.; Joshi, P.G.; Mishra, Y.K.; Khanna, P.K. Metal complexes driven from Schiff bases and semicarbazones for biomedical and allied applications: A review. *Mater. Today Chem.* **2019**, *14*, 100195. [[CrossRef](#)] [[PubMed](#)]
2. Vigato, P.A.; Peruzzo, V.; Tamburini, S. Acyclic and cyclic compartmental ligands: Recent results and perspectives. *Co-Ord. Chem. Rev.* **2012**, *256*, 953–1114. [[CrossRef](#)]
3. Bartyzel, A.; Kaczor, A. Synthesis, crystal structure, thermal, spectroscopic and theoretical studies of N3O2-donor Schiff base and its complex with Cu^{II} ions. *Polyhedron* **2018**, *139*, 271–281. [[CrossRef](#)]
4. Ermiş, E.; Durmuş, K. Novel thiophene-benzothiazole derivative azomethine and amine compounds: Microwave assisted synthesis, spectroscopic characterization, solvent effects on UV-Vis absorption and DFT. *J. Mol. Struct.* **2020**, *1217*, 128354. [[CrossRef](#)]
5. Rigamonti, L.; Cinti, A.; Forni, A.; Pasini, A.; Piovesana, O. Copper(II) complexes of tridentate Schiff Bases of 5-substituted salicylaldehydes and diamines—The role of the substituent and the diamine in the formation of mono-, di- and trinuclear species—Crystal structures and magnetic Properties. *Eur. J. Inorg. Chem.* **2008**, *23*, 3633–3647. [[CrossRef](#)]
6. Rigamonti, L.; Forni, A.; Pievo, R.; Reedijk, J.; Pasini, A. Copper(II) compounds with NNO tridentate Schiff base ligands: Effect of subtle variations in ligands on complex formation, structures and magnetic properties. *Inorg. Chim. Acta* **2012**, *387*, 373–382. [[CrossRef](#)]
7. Hegade, S.; Jadhav, Y.; Chavan, S.; Mulik, G.; Gautam, G. Catalytic assay of Schiff base Co(II), Ni(II), Cu(II) and Zn(II) complexes for N-alkylation of heterocycles with 1,3-dibromopropane. *J. Chem. Sci.* **2020**, *132*, 92–98. [[CrossRef](#)]
8. Shukla, N.S.; Gaur, P.; Bagri, S.S.; Mehrotra, R.; Chaurasia, B.; Raidas, M.L. Pd(II) complexes with ONN pincer ligand: Tailored synthesis, characterization, DFT, and catalytic activity toward the Suzuki-Miyaura reaction. *J. Mol. Struct.* **2021**, *1225*, 129071. [[CrossRef](#)]
9. Karman, M.; Romanowski, G. *Cis*-dioxidomolybdenum(VI) complexes with chiral tetradentate Schiff bases: Synthesis, spectroscopic characterization and catalytic activity in sulfoxidation and epoxidation. *Inorg. Chim. Acta* **2020**, *511*, 119832. [[CrossRef](#)]
10. Das, B.; Jana, A.; Mahapatra, A.D.; Chattopadhyay, D.; Dhara, A.; Mabhai, S.; Dey, S. Fluorescein derived Schiff base as fluorimetric zinc(II) sensor via ‘turn on’ response and its application in live cell imaging. *Spectrochim. Acta A* **2019**, *212*, 222–231. [[CrossRef](#)]
11. Oiyé, É.N.; Muzetti Ribeiro, M.F.; Toia Katayama, J.M.; Tadini, M.C.; Balbino, M.A.; Eleotério, I.C.; Magalhães, J.; Castro, A.S.; Mota Silva, R.S.; da Cruz Júnior, J.W.; et al. Electrochemical sensors containing Schiff bases and their transition metal complexes to detect analytes of forensic, pharmaceutical and environmental interest. A Review. *Crit. Rev. Anal. Chem.* **2019**, *49*, 488–509. [[CrossRef](#)] [[PubMed](#)]
12. Buta, I.; Ardelean, A.; Lönnecke, P.; Novitchi, G.; Hey-Hawkins, E.; Andruh, M.; Costisor, O. Structural and magnetic properties of three one-dimensional nitrate-, azido- and phenoxido-bridged copper(II) coordination polymers. *Polyhedron* **2020**, *190*, 114766. [[CrossRef](#)]

13. Rigamonti, L.; Forni, A.; Sironi, M.; Ponti, A.; Ferretti, A.M.; Baschieri, C.; Pasini, A. Experimental and theoretical investigations on magneto-structural correlation in trinuclear copper(II) hydroxido propellers. *Polyhedron* **2018**, *145*, 22–34. [[CrossRef](#)]
14. Zhang, S.; Deng, Q.; Zhang, H.; Zhang, S. Cobalt cubane clusters based on Schiff base: Synthesis, characterization, magnetic properties and Hirshfeld surface analysis. *J. Clust. Sci.* **2020**, *31*, 685–691. [[CrossRef](#)]
15. Gao, X.-S.; Ni, C.-C.; Ren, X.-M. Syntheses, crystal structures, photoluminescent and magnetic properties of complexes of zinc(II) and copper(II) with Schiff-base ligands derived from 2,6-diacetylpyridine. *Polyhedron* **2017**, *138*, 225–231. [[CrossRef](#)]
16. Gusev, A.N.; Kiskin, M.A.; Braga, E.V.; Chapran, M.; Wiosna-Salyga, G.; Baryshnikov, G.V.; Minaeva, V.A.; Minaev, B.F.; Ivaniuk, K.; Stakhira, P.; et al. Novel zinc complex with an ethylenediamine Schiff base for high-luminance blue fluorescent OLED applications. *J. Phys. Chem. C* **2019**, *123*, 11850–11859. [[CrossRef](#)]
17. Sutradhara, D.; Chowdhury, H.; Banerjee, S.; Sahad, N.M.; Ghosha, B.K. Syntheses, crystal structures and luminescence behaviors of four neutral penta-/hexacoordinate cadmium(II) compounds containing a tridentate Schiff base: Variation in coordination numbers, nuclearities and dimensionalities by changing halides/pseudohalides. *Inorg. Chim. Acta* **2019**, *485*, 86–97. [[CrossRef](#)]
18. Zheng, Z.-P.; Ou, Y.-J.; Hong, X.-J.; Wei, L.-M.; Wan, L.-T.; Zhou, W.-H.; Zhan, Q.-G.; Cai, Y.-P. Anion-dependent assembly of four sensitized near-infrared luminescent heteronuclear Zn^{II}–Yb^{III} Schiff base complexes from a trinuclear Zn^{II} complex. *Inorg. Chem.* **2014**, *53*, 9625–9632. [[CrossRef](#)]
19. Dong, Y.; Fan, R.-Q.; Chen, W.; Zhang, H.-J.; Song, Y.; Du, X.; Wang, P.; Wei, L.-G.; Fan, R. Different conjugated system Zn(II) Schiff base complexes: Supramolecular structure, luminescent properties, and applications in the PMMA-doped hybrid materials. *Dalton Trans.* **2017**, *46*, 1266–1276. [[CrossRef](#)]
20. Shiju, C.; Arish, D.; Kumaresan, S. Novel water soluble Schiff base metal complexes: Synthesis, characterization, antimicrobial-, DNA cleavage, and anticancer activity. *J. Mol. Struct.* **2020**, *1221*, 128770. [[CrossRef](#)]
21. Sangwan, V.; Singh, D.P. Macrocyclic Schiff base complexes as potent antimicrobial agents: Synthesis, characterization and biological studies. *Mater. Sci. Eng. C* **2019**, *105*, 110119. [[CrossRef](#)]
22. Laila, H.; Abdel-Rahman Ahmed, M.; Abu-Dief Emad, F.; Hamdan, S.K. Some new nano-sized Cr(III), Fe(II), Co(II), and Ni(II) complexes incorporating 2-((E)-(pyridine-2-ylimino)methyl)naphthalen-1-ol ligand: Structural characterization, electrochemical, antioxidant, antimicrobial, antiviral assessment and DNA interaction. *J. Photochem. Photobiol. B Biol.* **2016**, *160*, 18–31.
23. Laila, H.; Abdel-Rahman Ahmed, M.; Abu-Dief Maram Basha Azza, A.; Abdel-Mawgoud, A.A.H. Three novel Ni(II), VO(II) and Cr(III) mononuclear complexes encompassing potentially tridentate imine ligand: Synthesis, structural characterization, DNA interaction, antimicrobial evaluation and anticancer activity. *Appl. Organometal. Chem.* **2017**, *31*, 271–285.
24. Laila, H.; Abdel-Rahman Mohamed Shaker, S.; Adam Ahmed, M.; Abu-Dief, H.; Moustafa Maram, T.; Basha Ahmed, S.; Ahmed, H.E.-S. Synthesis, theoretical investigations, biocidal screening, DNA binding, in vitro cytotoxicity and molecular docking of novel Cu (II), Pd (II) and Ag (I) complexes of chlorobenzylidene Schiff base: Promising antibiotic and anticancer agents. *Appl. Organometal. Chem.* **2018**, *32*, 527–535.
25. Laila, H.; Abdel-Rahman Ahmed, M.; Abu-Dief Mohamed, R.; Shehata Faten, M.; Atlam Azza, A.; Abdel-Mawgoud, H. Some new Ag(I), VO(II) and Pd(II) chelates incorporating tridentate imine ligand: Design, synthesis, structure elucidation, density functional theory calculations for DNA interaction, antimicrobial and anticancer activities and molecular docking studies. *Appl. Organometal. Chem.* **2019**, *33*, 4699–4708.
26. Ahmed, M.; Abu-Dief Laila, H.; Abdel-Rahman Azza, A.; Abdel-Mawgoud, H. A robust in vitro Anticancer, Antioxidant and Antimicrobial Agents Based on New Metal-Azomethine Chelates Incorporating Ag(I), Pd (II) and VO (II) Cations: Probing the Aspects of DNA Interaction. *Appl. Organometal. Chem.* **2020**, *34*, 1–13.
27. Groom, C.R.; Bruno, I.J.; Lightfoot, M.P.; Ward, S.C. The Cambridge Structural Database. *Acta Cryst.* **2016**, *B72*, 171–179. [[CrossRef](#)]
28. Li, S.L.; Liu, L.; Xu, Q.T.; Jiang, H.H.; Li, D.; Líu, D.X.; Chen, S.H.; Yang, Z.H. Crystal structure of a mixed ligand trinuclear complex of cadmium(II). *J. Coord. Chem.* **1998**, *46*, 97–104. [[CrossRef](#)]
29. Mukherjee, A.; Rudra, I.; Naik, S.G.; Ramasesha, S.; Nethaji, M.; Chakravarty, A.R. Covalent linkage of the type-2 and type-3 structural mimics to model the active site structure of multicopper oxidases: Synthesis and magneto-structural properties of two angular trinuclear copper(II) complexes. *Inorg. Chem.* **2003**, *42*, 5660–5668. [[CrossRef](#)]

30. Yang, F.-L.; Shao, F.; Zhu, G.-Z.; Shi, Y.-H.; Gao, F.; Li, X.-L. Structures and magnetostructural correlation analyses for two novel hexanuclear complexes based on a pentadentate Schiff base ligand. *Chem. Sel.* **2017**, *2*, 110–117. [CrossRef]
31. Dolai, M.; Mistri, T.; Panja, A.; Ali, M. Diversity in supramolecular self-assembly through hydrogen-bonding interactions of non-coordinated aliphatic –OH group in a series of heterodinuclear Cu^{II}M (M = Na^I, Zn^{II}, Hg^{II}, Sm^{III}, Bi^{III}, Pb^{II} and Cd^{II}). *Inorg. Chim. Acta* **2013**, *399*, 95–104. [CrossRef]
32. Bartyzel, A. Synthesis, thermal behaviour and some properties of Cu^{II} complexes with N,O-donor Schiff bases. *J. Therm. Anal. Cal.* **2018**, *131*, 1221–1236. [CrossRef]
33. Agilent Technologies Ltd. *CrysAlis PRO*; Agilent Technologies Ltd.: Oxfordshire, UK, 2014.
34. Sheldrick, G.M. Crystal structure refinement with SHELXL. *Acta Cryst.* **2015**, *C71*, 3–8.
35. Farrugia, L.J. WinGX and ORTEP for Windows: An update. *J. Appl. Cryst.* **2012**, *45*, 849–854. [CrossRef]
36. Macrae, C.F.; Sovago, I.; Cottrell, S.J.; Galek, P.T.A.; McCabe, P.; Pidcock, E.; Platings, M.; Shields, G.P.; Stevens, J.S.; Towler, M.; et al. Mercury 4.0: From visualization to analysis, design and prediction. *J. Appl. Cryst.* **2020**, *53*, 226–235. [CrossRef]
37. Spek, A. Single-crystal structure validation with the program PLATON. *J. Appl. Crystallogr.* **2003**, *36*, 7–13. [CrossRef]
38. Raman, N.; Pothiraj, K.; Baskaran, T. DNA interaction, antimicrobial, electrochemical and spectroscopic studies of metal(II) complexes with tridentate heterocyclic Schiff base derived from 20-methylacetoacetanilide. *J. Mol. Struct.* **2011**, *1000*, 135–144. [CrossRef]
39. Deelod, W.; Wannapaiboon, S.; Pansiri, P.; Kumpeerakij, P.; Phomphrai, K.; Laobuthee, A.; Hanlumyung, Y.; Suramit, S.; Piyanut, P.; Worawat, W. Crystal structure and Hirshfeld surface analysis of bis(triethanolamine)nickel(II) dinitrate complex and a revelation of its characteristics via spectroscopic, electrochemical and DFT studies towards a promising precursor for metal oxides synthesis. *Crystals* **2020**, *10*, 474. [CrossRef]
40. Ignatyev, I.; Kondratenko, Y.; Fundamensky, V.; Kochina, T. Synthesis and characterization of cobalt(II) complexes with triethanolamine and succinate and/or nitrate anions. *Transit. Met. Chem.* **2017**, *43*, 127–136. [CrossRef]
41. Nakamoto, K. *Infrared and Raman Spectra of Inorganic and Coordination Compounds Part B: Applications in Coordination, Organometallic, and Bioinorganic Chemistry*, 6th ed.; John Wiley & Sons: Hoboken, NJ, USA, 2006.
42. Yang, L.; Powell, D.R.; Houser, R.P. Structural variation in copper(I) complexes with pyridylmethylamide ligands: Structural analysis with a new four-coordinate geometry index, τ_4 . *Dalton Trans.* **2007**, *9*, 955–964. [CrossRef]
43. Okuniewski, A.; Rosiak, D.; Chojnacki, J.; Becker, B. Coordination polymers and molecular structures among complexes of mercury(II) halides with selected 1-benzoylthioureas. *Polyhedron* **2015**, *90*, 47–57. [CrossRef]
44. Addison, A.W.; Rao, N.T.; Reedijk, J.; van Rijn, J.; Verschoor, G.C. Synthesis, structure, and spectroscopic properties of copper(II) compounds containing nitrogen–sulphur donor ligands; the crystal and molecular structure of aqua [1,7-bis(N-methylbenzimidazol-2'-yl)-2,6-dithiaheptane]copper(II) perchlorate. *J. Chem. Soc. Dalton Trans.* **1984**, *7*, 1349–1356. [CrossRef]
45. Mukherjee, A.; Saha, M.K.; Rudra, I.; Ramasesha, S.; Nethaji, M.; Chakravarty, A.R. Synthesis, crystal structure and magnetic properties of quasi-linear tetranuclear copper(II) Schiff base complexes formed by covalent linkage of asymmetrically bridged dicopper(II) units. *Inorg. Chim. Acta* **2004**, *357*, 1077–1082. [CrossRef]
46. Thermo Scientific. *Nicolet TGA Vapor Phase, FTIR Spectra Library by Software OMNIC*; Thermo Scientific: Waltham, MA, USA, 2007.

Publisher's Note: MDPI stays neutral with regard to jurisdictional claims in published maps and institutional affiliations.



© 2020 by the authors. Licensee MDPI, Basel, Switzerland. This article is an open access article distributed under the terms and conditions of the Creative Commons Attribution (CC BY) license (<http://creativecommons.org/licenses/by/4.0/>).